Tensile stress relaxation and recovery behavior of a cross-linked EPDM rubber matrix loaded with different fillers

Françoise Ehrburger-Dolle, Isabelle Morfin, Françoise Bley, Frédéric Livet, Gert Heinrich, Luc Piché, Mark Sutton

Tensile stress relaxation and recovery behavior of a cross-linked EPDM rubber matrix loaded with different fillers

Françoise Ehrburger-Dolle[*1], Isabelle Morfin[1], Françoise Bley[2], Frédéric Livet[2], Gert Heinrich[3], Luc Piché[4], Mark Sutton[4]*

[1]Univ. Grenoble 1 / CNRS, LIPhy UMR 5588, Grenoble, F-38041, France

[2]SIMaP, UMR 5266 Grenoble INP / CNRS / UJF, 38402 Saint Martin d'Hères, France

[3]Leibniz-Institut für Polymerforschung Dresden, 010169 Dresden, Germany

[4]Physics Department, McGill University, Montreal, Quebec H3A 2T8, Canada

ABSTRACT. Tensile stress-relaxation measurements have been performed on a series of cross-linked filled elastomers. The samples are constituted by the same Ethylene-Propylene-Diene-Monomer (EPDM) matrix. The different fillers are chosen in order to investigate the effect of the filler-filler and the filler-matrix interactions on the time dependence of the relaxation modulus $E(t)$ at different strain values ε during about 4000 s. Each strain step is reached by a change of strain Δε that is positive during the first (UP1) and the second (UP2) elongation or negative (DOWN) when the strain plateaus are decreased. Analysis of the experimental data indicates that most of the curves obtained after a positive strain change (UP1 or UP2) yielding a decrease of $E(t)$, can be fitted by the empirical Chasset-Thirion equation $E(t) = E_\infty[1 + (t/\tau_0)^{-m}]$. For

carbon black samples characterized by a strong filler-matrix interaction, the value of the exponent *m* may become very small and the data are better fitted by a logarithmic relation $E(t) = E(1)[1 - K\log(t)]$. As for the increase of $E(t)$ measured after a negative strain step (DOWN), it is shown, for the first time, that all data can be fitted by the following equation: $E(t) = E_\infty[1 - (t/\tau_0)^{-m}]$. This result allows us to introduce a generalized Chasset-Thirion equation writing $E(t) = E_\infty[1 + k(t/\tau_0)^{-m}]$ in which $k = 1$ when Δε is positive and $k = -1$ when Δε is negative. It is suggested that the physical meaning of the exponent *m* stemming from the generalized Chasset-Thirion equation can be assimilated to the exponent $x - 1$ in the soft glassy rheology (SGR) model.

1 INTRODUCTION

The mechanical behavior of filled elastomers is an active research area since more than 50 years mainly because it is related to an ancient and important application which is the reinforcement of rubber. Several recent reviews in the literature provide information about new developments in the field of polymer nanocomposites. Basic principles and technological applications have been reviewed by Vilgis et al. [1] and Heinrich et al. [2]. The latest advances in the viscoelastic behavior of rubbery materials were described and analyzed by C. M. Roland [3]. A recent book [4] is dealing about preparation, properties and applications of rubber nanocomposites. A review dealing with structure, phase behavior and properties of nanocomposites has been published by Kumar and Krishnamoorti [5]. Oberdisse et al. [6] reported recent investigations devoted to the determination of the structure of polymer nanocomposites by means of small-angle scattering techniques. A survey of the present understanding of polymer-based nanocomposites as obtained from either theoretical or computational approaches was presented by Allegra et al. [7].

The mechanical behavior of filled elastomers is characterized by two major features. The first one concerns the non-linear viscoelastic behavior (or Payne effect) revealed by the amplitude dependence of the storage and the loss moduli in shear or tensile measurements [8-10]. The second one is stress-softening (or Mullins effect) yielding the lowering of the resulting stress for the same applied strain after the first load and, as a consequence, mechanical hysteresis. The Mullins effect was recently reviewed by Diani et al. [11] and Amin et al. [12]. Bhattacharya *et al*. [13] reviewed several "classical" models attempting to take into account the complexity of the problem. These authors also reported an extensive study of the nonlinear, time-dependent mechanical behavior of a cross-linked carbon black filled elastomer. The unusual non-linear and plastic behavior of nanofilled elastomers was recently attributed to kinetics of rupture and re-birth of glassy bridges [14-16]. Resting time and relaxation features are also involved in partial [17] or complete [18, 19] recovery (or healing) of the Mullins effect at room temperature.

Early measurements of tensile stress relaxation in a series of carbon black N330 filled rubber vulcanizates were reported by MacKenzie and Scalan [20]. The experimental data could be fitted almost equivalently either by a logarithmic function of time or a power law with exponents smaller than 0.07. The authors produced evidences for the existence of a distinct relaxation process below 60 seconds that vanished above a given strain, depending on the amount of filler. Similar results were obtained for vulcanized ethylene-propylene-diene-monomer (EPDM) rubber filled with carbon black N660 [21]. Geethamma et al. [22] showed that the slope of the lines obtained in semi-logarithmic coordinates was larger for plain natural rubber (NR) than for filled ones. The increase of the amount of filler consisting of short coir fibers lead to the decrease of the absolute value of the slope. Opposite features were reported for NR filled with titania or silica particles [23]. In the case of nanogel filled elastomers, Mitra et al. [24] fitted the

experimental values of the relaxation modulus with power laws in which the exponents varied between 0.2 and 0.3. More precisely, these authors used the following equation:

$$E(t) = E_\infty[1 + (t/\tau_0)^{-m}] \quad (1)$$

which has been proposed in 1965 by Chasset and Thirion [25] for describing the isothermal tensile relaxation modulus data $E(t)$ for many rubbers. In this equation, E_∞ is the equilibrium modulus and τ_0 and m are parameters which depend on the system investigated. The same equation applies also to the shear modulus relaxation $G(t)$

$$G(t) = G_\infty[1 + (t/\tau_0)^{-m}] \quad (2)$$

An analogous equation was used by Dickie and Ferry [26] for fitting the creep compliance relaxation $J(t) = 1/G(t)$ in dicumyl peroxide vulcanizated natural rubbers. The Chasset-Thirion (CT) equation has been widely used to describe power law stress relaxation in unfilled polymers or elastomers [27, 28-32]. In several cases, the exponent m was shown to increase linearly with the cross-linking density. Theoretical models have been proposed by Curro et al [33, 34] and Heinrich and Vilgis [35] for explaining this feature and for justifying a posteriori the CT equation. However, several authors have shown that the linearity of the relation between m and the cross-linking density fails, as in the case of end-linked polydimethylsiloxane (PDMS) elastomers with pendent chains [27]. More, a decrease of m when the cross-linking density increases was reported by Martin et al. [30] for EPDM networks cross-linked with resol under compressive strain at 100°C.

In fact, there are many classes of materials in which stress relaxation is not exponential but best represented as log(t) [36] or as a power law in time [37]. Examples of such materials include,

among others, block copolymers [38] and, more generally foams, emulsions, soft colloidal glasses, food products and others [37]. Power-law stress relaxation implies also power-law behavior in the frequency-dependence of the viscoelastic storage $G'(\omega)$ and loss $G''(\omega)$ moduli in materials for which there is no single characteristic relaxation time. Similarities in the rheology of many soft materials led Sollich and coworkers [39-41] to propose the soft glassy rheology (SGR) model. Moreover, SGR features are also observed in many biological systems [42-50]. It appears, however, that the elementary biophysical and biochemical mechanisms which govern the cell mechanics may not be well described by the SGR model. Therefore, other models involving a broad distribution of relaxation times were proposed [48] to explain power law relaxation. Jaishankar and McKinley [37] presented recently a constitutive framework using fractional derivatives to model the power-law responses observed experimentally in very different complex systems. These authors also show that the "effective noise temperature" x appearing in the exponent $x - 1$ in the SRG model is intimately related to the exponents involved in their fractional model.

This non-exhaustive bibliographic survey concerning stress relaxation or recovery processes suggests that the power law involved in the CT equation could not be limited to the particular situation of cross-linked elastomers. It follows also that the physical meaning of the exponent m could be different from that involved in the Curro model since the power law behavior is typical of structural disorder and metastability [37, 39-41] and implies a broad distribution of relaxation times. We have shown in a recent paper [51] that the decrease of the force $F(t)$ requested to maintain an elongation of 60% of cross-linked silica filled elastomer can be fitted by a power law equation formally similar to the CT equation and an exponent equal to 0.17. In the case of a cross-linked carbon black filled elastomer, under the same conditions, the force decreases as

log(t). Heterodyne X-ray photon correlation spectroscopy (HD-XPCS) measurements performed simultaneously revealed a significant difference in the value of the velocity of the filler particles. For the carbon black filled sample, the logarithmic decrease of the tensile force was associated with a small velocity of the filler particles that decreased rapidly with time. These features would agree with the concept of glassy bridges in filled elastomers [14-16]. On the opposite, for the hydroxylated silica sample, the aggregate velocity was about 10 times larger than that of the carbon black ones and its decrease with time was slower. These measurements suggested (i), similarities between the behavior of the silica filled sample and that of colloidal gels or soft glasses [52] [53] and (ii) the absence of glassy domains as also observed in other silica filled elastomers [54-56]. This paper also emphasized the effect of the filler-filler (strong for hydroxylated silica fillers) and the filler-matrix (strong for carbon black fillers after cross-linking of the matrix [57]) interactions on the stress relaxation behavior of nanocomposites at the macroscopic and at the mesoscopic scale.

Progresses in fundamental knowledge on polymer-particle interaction and its link with macroscopic properties were recently reviewed by Pandey et al. [58]. Lin et al. [59] investigated the role of the nanofillers on the polymer dynamics in order to get new insights into understanding processing conditions and rheological behavior of polymer nanocomposites. The work described in the present paper was performed with similar objectives. Its aim is to show that the behavior of the relaxation and recovery of filled elastomers may provide a link between macroscale mechanical features and nanoscale polymer-filler interaction. This link could be the power law exponent m (or more precisely, the value of $m + 1$). To this end a well-defined series of samples have been prepared. They consist of the same Ethylene Propylene Diene Monomer (EPDM) cross-linked rubber filled with an hydroxylated silica (strong filler-filler interaction), an

hydrophobic silica having the same morphology (intermediate filler-filler and filler matrix interaction) and carbon black (strong filler matrix interaction) at two different concentrations. In order to determine the tensile relaxation and recovery (under strain), measurements were performed at different steps of strain ε_f reached after a positive step increase $\Delta\varepsilon = \varepsilon_f - \varepsilon_i$ where $\varepsilon_f > \varepsilon_i$ and ε_i being the initial strain or a negative step $\Delta\varepsilon$ where $\varepsilon_f < \varepsilon_i$. Tensile relaxation was also measured during the second increase of strain in order to get new information about the Mullins effect. Relevancy of the SRG model to strained filled elastomers will be discussed in the last paragraph.

2. MATERIALS AND EXPERIMENTAL METHODS

2.1 Samples. The elastomer matrix investigated is an Ethylene Propylene Diene Monomer (EPDM) rubber (Buna EP G 6850, Lanxess, Leverkusen, Germany). Three different fillers were used: carbon black N330 (Evonik Carbon Black GmbH), hydroxylated pyrogenic silica AEROSIL® 200 (Degussa) and AEROSIL® R 974. The latter is a hydrophobic fumed silica aftertreated with dimethyldichlorosilane based on the hydrophilic AEROSIL® 200 with a specific surface area close to 200 m^2/g. The morphological characteristics of the fillers have been previously described in details [60-62]. The filled elastomers were prepared by mixing 20 or 40 g of filler with 100 g of rubber (i.e., 20 or 40 phr) and 3 g of dicumyl peroxide (the cross-linking agent) in a two-roll mill for 5 minutes at 50°C. Afterwards, the mixtures were cured in molds at 160°C under pressure during 10 minutes. The volume fraction of filler ϕ corresponding to 40 phr is close to 0.16 for the carbon black filled sample and to 0.14 for the silica ones. In both cases, the volume fraction is expected to be above the "percolation" threshold which is close to 0.10 for carbon black N330 [63] and 0.02 for AEROSIL® 200 [64, 65]. At 20 phr, the volume fraction is

slightly below percolation for carbon black (ϕ=0.09) but probably above percolation, for silica (ϕ=0.07). In the following, the names Si-OH-40-c, Si-OR-40-c and CB-40-c will refer to cross-linked samples with 40 phr of AEROSIL® 200, AEROSIL® R 974 and carbon black, respectively. Samples with 20 phr will be named Si-OH-20-c, Si-OR-20-c and CB-20-c. The uncross-linked AEROSIL® 200 filled sample will be named Si-OH-40-u.

The thickness *e* of the samples used for the stress-strain measurements was about 2 mm. For the tensile stress relaxation, *e* was equal to1 mm. For all measurements, the one or two millimeter thick plates were punched out to the classical dumb-bell shape. The width *l* of the gauge ranged between 4 and 4.2 mm depending on the puncher used. Its length was equal to 25 mm.

2.2 Tensile force measurements. The tensile stress-elongation curves (monotonous stress-strain curves) were measured according ISO 527-2 with a universal testing machine Zwicki Z2.5. at the IPF in Dresden using S2 specimen geometry. The stretch ratio λ is defined as $\lambda = L/L_0$ where L and L_0 are the final and the initial lengths respectively. The strain ε is defined as $\varepsilon = (L - L_0)/L_0 = \lambda - 1$ (engineering strain). The strain rate $d\varepsilon/dt$ was equal to 0.133 s^{-1} corresponding to a crosshead speed of 200 mm/min and initial clamping length of 25 mm. Tensile relaxation measurements performed at given steps of strain (incremental stress-strain curves) were achieved by means of the apparatus designed for simultaneous stress and XPCS study [51]. A complete description can be found in the master thesis of L.J.S. Halloran [66]. Each strain step was reached after a rapid extension (0.034 s^{-1}) from the previous step to the next one. A strain gauge and a digitizing unit were used to measure the evolution of the force *F* every 1 or 2 s at each elongation step. The value of the stress σ is deduced from *F* by $\sigma = F/A$ where $A = el$ is the section of the sample. The tensile relaxation modulus $E(t)$ is defined as $E(t) =$

$\sigma(t)/\varepsilon$. Fitting of the experimental curves is achieved by non-linear regression procedures by means of the Marquardt - Levenberg algorithm provided by SigmaPlot 10.0.

3. ANALYSIS OF THE STRESS-STRAIN CURVES

3.1. Monotonous stress-strain curves. Figure 1a shows the variation of the stress σ as a function of the strain ε plotted in logarithmic coordinates for all samples. In the small elongation domain, all curves exhibit a power law behavior $\sigma(\varepsilon) = \sigma_0 \varepsilon^n$. The value of the exponent *n* is nearly the same for all curves ($n = 0.75 \pm 0.02$). The domain in which this power law is verified, however, is not exactly the same for all samples. For the plain EPDM elastomer the power law is observed for ε values ranging between 0.03 and 0.26. ($0.03 < \varepsilon < 0.26$) For the CB filled samples, the limits are 0.015 and 0.14. In the case of the silica samples, the limits of the power law domain are shifted to smaller (0.004 to 0.06) ε values for Si-OH-40-c or the domain becomes narrower (0.02 to 0.06) for Si-OR-40-c. In the region of small strains, a linear variation of σ with ε corresponding to an elastic deformation is expected. Thus, the slope *n* of the logarithmic plots shown in Figure 1a should be equal to 1. Because tensile stress-strain data obtained for filled elastomers are never plotted in logarithmic coordinates, it is difficult to determine whether or not such non-linear effect was already reported. Power law relationships can be found in the case of uniaxial tensile tests on metals and alloys (Hollomon equation) [67, 68]. In the case of polymeric materials [69] or fiber composites under elongation [70] or under compression [71], high strain rates induce viscoplasticity. From this non-exhaustive list of publications it can be concluded that the stress-strain power law behavior observed at small deformations could reveal plastic or elastoplastic effects, i.e., structural damages or failures. The existence or not of a relation between a power law behavior and the hysteresis associated to

strain-softening characteristic of the Mullins effect would require further investigations. Thus, the origin of the power-law behavior shown in Figure 1a can hardly be found without further experimental work. The fact that the value of the exponent is nearly the same for all samples suggests that the hot-pressing step common to all samples, could induce a particular internal structure that would be almost irreversibly destroyed during the first stretch. It is worth mentioning the occurrence of plastic events in model polymeric glasses at very small strains, in a regime where the material is generally described as elastic [72].

The existence of a power law domain at small elongations allows us to calculate the relative stress σ_r by dividing the experimental values $\sigma(\varepsilon)$ by the prefactor σ_0. The collapsed curves plotted in Figure 1b reveal differences in the mechanical behavior of the samples at larger ε values. The first comment concerns the two CB samples: up to $\varepsilon \approx 0.7$ the increase of the stress is nearly similar to that of the un-filled cross-linked elastomer. Thus it may be assumed that the carbon black particles act as additional cross-links. At larger strains, the shape of the curves indicates that stiffening occurs without the foregoing of a well-defined yield region.

On the opposite, for the OH-silica filled sample Si-OH-40-c that appears to be the stiffest at small strains, there is a well-defined yield region corresponding to strain softening. It is likely that this effect results from a progressive opening of interparticle H-bonds in the silica network. Figure 1b shows that the relative strain softening effect decreases when the amount of OH-silica decreases from 40 to 20 phr.

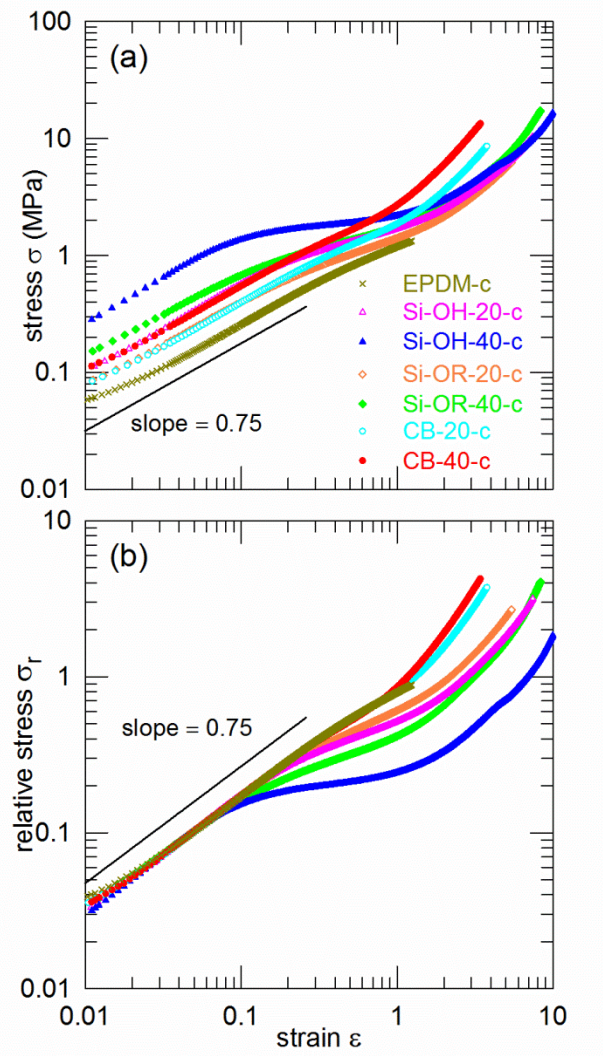

Figure 1. Stress-strain curves measured at a constant strain rate (0.133 s^{-1}) (a) and (b), relative stress $\sigma_r(\varepsilon) = \sigma(\varepsilon)/\sigma_0$ plotted in logarithmic coordinates.

3.2. Incremental stress-strain curves. The curves obtained for the different samples are shown in Figure 2. In all cases, the difference between each strain step is equal to 0.2. The maximum strain is 0.6 for Si-OR-20-c, Si-OH-40-c and CB-40-c. For the 3 other samples, the limit is 0.8. Sample Si-OR-20-c broke during the second elongation (UP2) at 0.6.

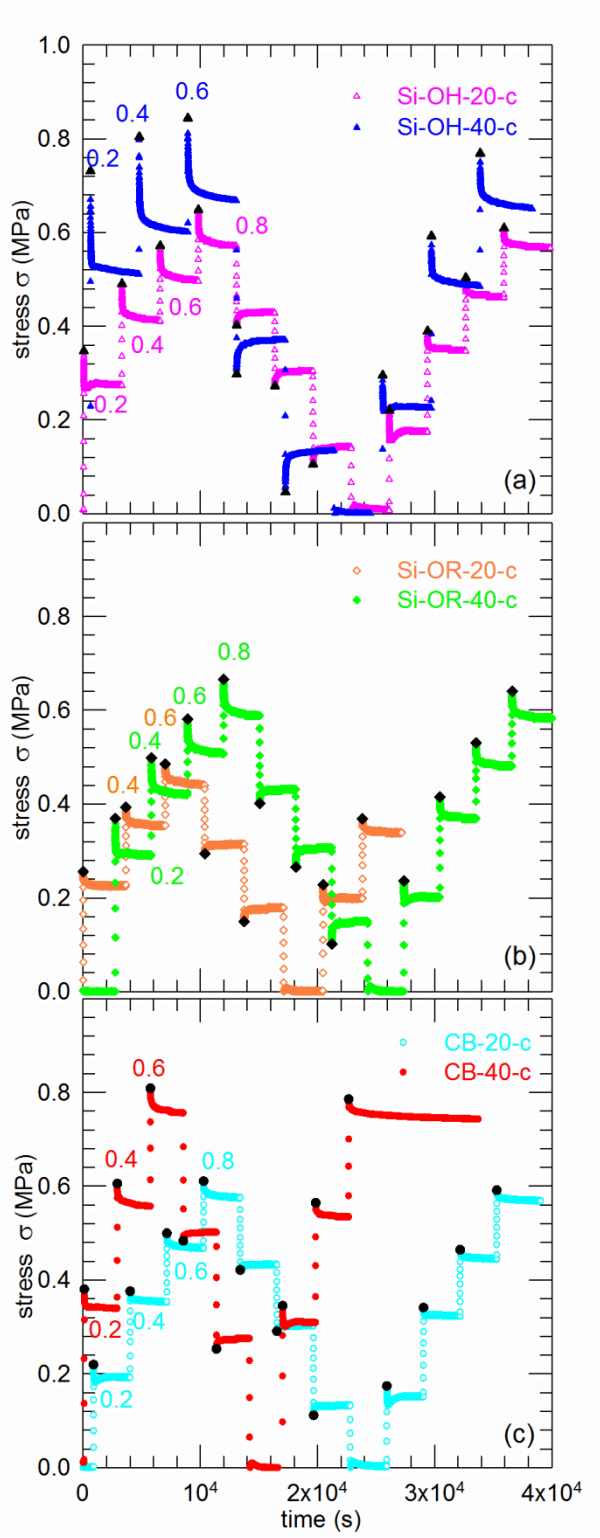

Figure 2 (a, b, c). Incremental stress-strain curves. The filled black symbols correspond to the origin (t=0) of the time scale in the aging curves.

3.3. Comparison between monotonous and incremental stress strain curves. Figure 2 indicates that the value of the maximum of the stress at each step is systematically smaller than that measured at the same strain shown in Figure 1a. This result may be explained by the fact that the change from one strain step to the next one is slower (0.034 s^{-1}) than the continuous increase of strain (0.133 s^{-1}) [73]. It appears (Figure 3a) that the two series of data are simply related by a multiplying factor for strain values between 0.2 and 0.6. It follows that the mechanism of the increase of stress with strain is the same in both cases in the 0.2-0.6 strain range. Above 0.6, the stress seems to be slightly overestimated. Furthermore, the stress values measured for CB-40-c by strain steps equal to 0.2 and 0.1 (open and closed circles in Figure 3, respectively) are nearly the same.

Figure 3b shows the evolution with strain of the tensile modulus $E(\varepsilon) = \sigma(\varepsilon)/\varepsilon$. In the investigation of the tensile relaxation modulus $E(t)$ at a given ε, presented in the next paragraphs, the data point shown in this figure correspond to the initial values named $E(0)$ (after suppression of the shifting factor introduced in the plots). This figure indicates that the amplitude of the decrease of the tensile modulus is significantly larger for the hydroxylated silica filled sample (Si-OH-40-c) than for the carbon black filled one (CB-40-c). For the other samples, the amplitude of the decrease stays between these two limits, as it is also shown in Figure 1b.

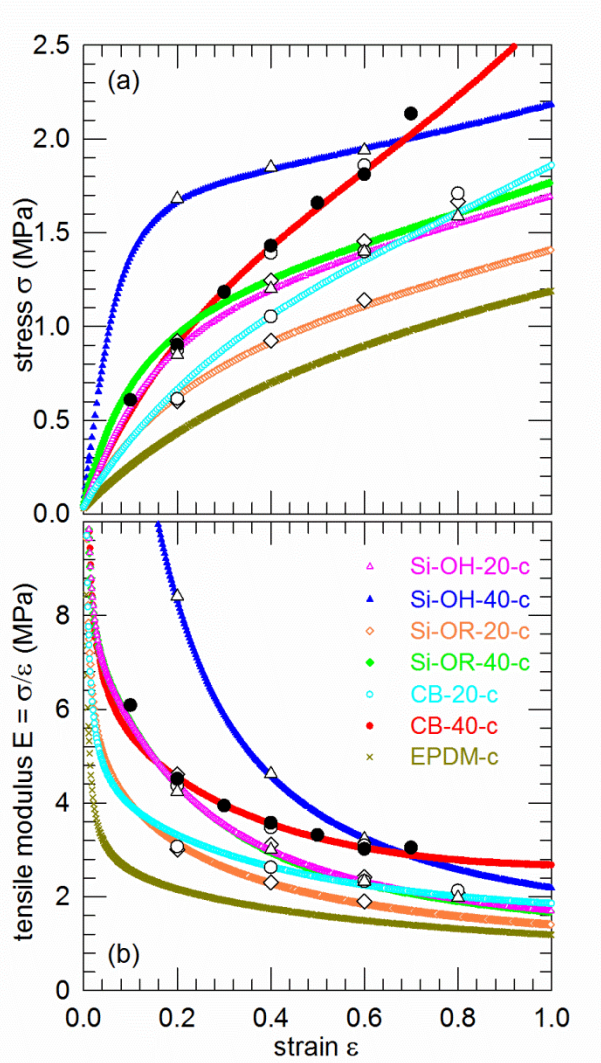

Figure 3. Comparison between stress (a) and tensile modulus (b) data obtained during the monotonous (Figure 1) and the incremental (Figure 2) measurements. The black open symbols correspond to the points shown in Figure 2 (first stretch) after multiplication by a factor ranging between 2.2 and 2.5. The black closed symbols correspond to the values of the stress measured for CB-40-c with a step interval equal to 0.1.

4. ANALYSIS OF THE TENSILE RELAXATION MODULUS DATA

4.1. Experimental results obtained for ε = 0.40. The time dependence of the tensile relaxation modulus $E(t) = \sigma(t)/\varepsilon$ is measured during the first (UP1) and the second step (UP2) of strain reached from below ($\Delta\varepsilon > 0$) and for the same strain step reached from above (DOWN, $\Delta\varepsilon < 0$) as shown in Figure 2. The results obtained for ε = 0.40 are plotted in Figure 4. They are grouped within three graphs corresponding to the hydroxylated silica filler (Si-OH-c), the hydrophobic one (Si-OR-c) and the carbon black filler (CB-c) at 20 and 40 phr respectively. These graphs indicate that the overall amplitude of the variations of $E(t)$ becomes smaller when going from graph (a) to graph (c). For the CB-c samples (Figure 4c), the 3 curves (UP1, DOWN and UP2) obtained for the samples containing 20 phr are clearly separated from the ones obtained for 40 phr. Furthermore, for CB-40-c (UP1), the concavity is directed towards the time axis while for all other UP curves, it is the convexity. For the latter, the Chasset-Thirion (CT) equation (Equation 1) properly fits the experimental data for $t \geq 1$ s as shown in Figure 4. The values of the parameters deduced from the fits collected in Table 1 will be discussed in paragraph 5. We have observed that the experimental values $E(0)$ are systematically very close to $E(1)$ calculated by using the fitting equation (Equation 1).

As for the data obtained for CB-40-c (UP1), the empirical fitting equation becomes:

$$E^*(t) = E(0)[1 - (t/\tau_0)^{-m}] \qquad (3)$$

with $m < 0$ as shown in Table 1. It follows that $E(t)$ decreases from the initial value $E(0)$ without reaching an asymptotic equilibrium value (E_∞) as it is the cases for the other UP curves shown in Figure 4.This feature could suggest the occurrence of plastic effects (damages).

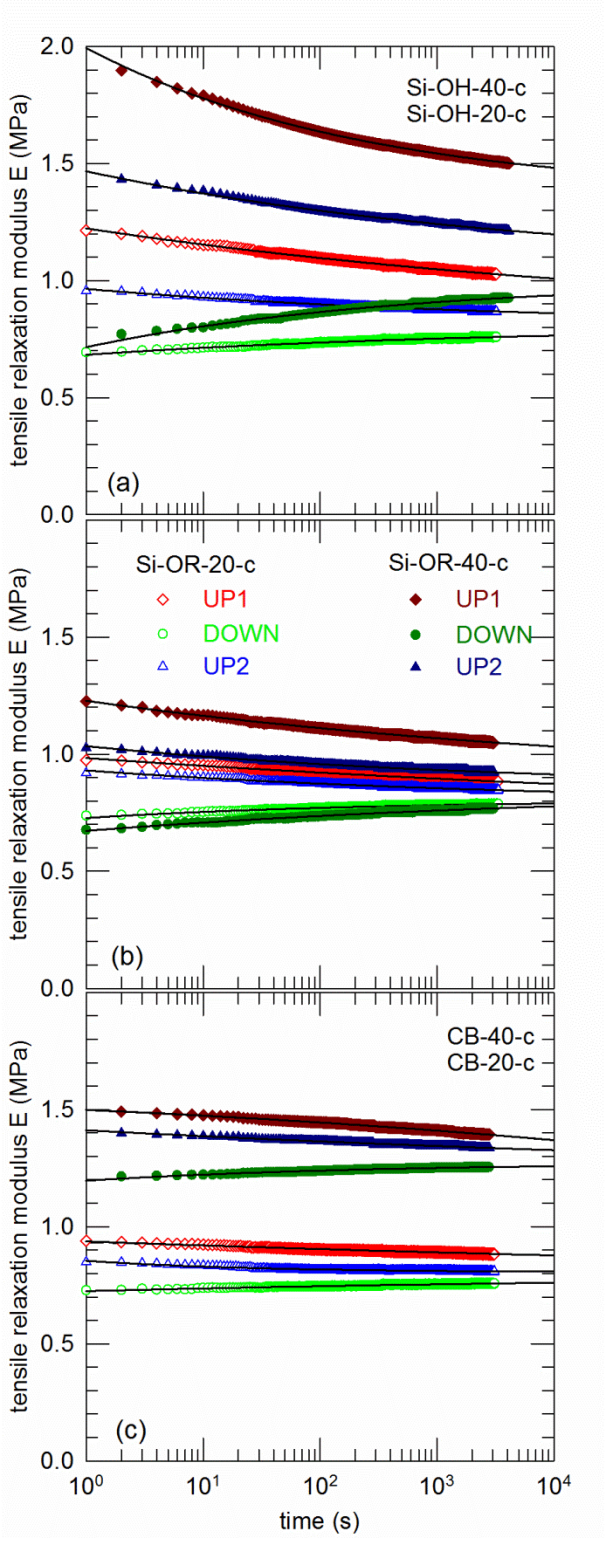

Figure 4. Time dependence of the tensile relaxation modulus *E* for ε = 0.40. (a) series Si-OH-c samples, (b) series Si-OR-c samples and (c) series CB-c samples.

ε = 0.4		E(0) (MPa)	E_∞ (MPa)	*m*	τ_0 (s)
Si-OH-20-c	UP1	1.226	0.811 ± 0.005	0.080 ± 0.002	$(2.0 \pm 0.1)\times10^{-4}$
	DOWN#	0.681	0.803 ± 0.002	0.125 ± 0.004	$(2 \pm 1)\times10^{-7}$
	UP2	0.973	0.812 ± 0.003	0.124 ± 0.004	$(1.4 \pm 0.5)\times10^{-6}$
Si-OH-40-c	UP1	2.010	1.364 ± 0.001	0.182 ± 0.001	0.0143 ± 0.0002
	DOWN#	0.744	1.000 ± 0.002	0.163 ± 0.003	$(4.5 \pm 0.6)\times10^{-4}$
	UP2	1.480	1.047 ± 0.004	0.111 ± 0.002	$(2.7 \pm 0.2)\times10^{-4}$
Si-OR-20-c	UP1	0.983	0.70 ± 0.01	0.054 ± 0.003	$(4.5 \pm 0.3)\times10^{-8}$
	DOWN#	0.735	0.803 ± 0.001	0.180 ± 0.004	$(2.4 \pm 0.7)\times10^{-6}$
	UP2	0.922	0.786 ± 0.003	0.107 ± 0.004	$(1.4 \pm 0.6)\times10^{-7}$
Si-OR-40-c	UP1	1.246	0.871 ± 0.004	0.086 ± 0.002	$(3.1 \pm 0.1)\times10^{-5}$
	DOWN#	0.664	0.853 ± 0.005	0.094 ± 0.004	$(7 \pm 4)\times10^{-8}$
	UP2	1.038	0.856 ± 0.003	0.122 ± 0.004	$(2.7 \pm 0.8)\times10^{-6}$
CB-20-c	UP1	0.940	0.74 ± 0.02	0.038 ± 0.004	$\approx 10^{-15}$
	DOWN#	0.727	0.791 ± 0.003	0.084 ± 0.006	$\approx 10^{-13}$
	UP2	0.853	0.805 ± 0.001	0.304 ± 0.006	$(1.1 \pm 0.2)\times10^{-4}$
CB-40-c	UP1#	1.514	*E_0=1.63 ± 0.01*	*-0.074± 0.003*	*$\approx 10^{15}$*
	DOWN#	1.209	1.273 ± 0.001	0.117 ± 0.004	$(1.3 \pm 0.4)\times10^{-7}$
	UP2	1.411	1.19 ± 0.02	0.053 ± 0.005	$\approx 10^{-14}$

Table 1. Parameters deduced from the fit of the data shown in Figure 4 by Equations (5). The sign # indicates $k = -1$ in Equation (5).

When the strain step is negative *i. e.*, when the strain is decreased from ε = 0.60 to 0.40 (DOWN curves), $E(t)$ increases with time. It appears that all data (including CB-40-c) can be properly fitted by using the following equation:

$$E^{\#}(t) = E_{\infty}[1 - (t/\tau_0)^{-m}] \qquad \text{with } m > 0 \qquad (4)$$

To the best of our knowledge, such a modified CT equation has never been proposed for fitting the after-strain recovery. The recovery process was often described by kinetic aggregate breaking and reforming (flocculation) [74-76] described by exponential equations. In fact, figure 4 shows that the approach of the tensile relaxation modulus $E(t)$ to a steady state differs depending upon the direction of the change in the strain amplitude as observed earlier by Wang and Robertson **[**77**]**. These authors considered this asymmetry as one of the evidences of the existence of an analogy between strain-induced nonlinearity in the modulus of filled rubbers, the physics of the glass transition of glass-forming materials, and the jamming transition of vibrated granular materials. As a consequence, the asymmetric behavior cannot be interpreted by simple kinetic models. It seems now that the modified CT equation could capture the physical meaning of the unusual phenomena observed in filled rubbers.

These features which will be discussed in more details in paragraph 5, allow us to introduce an alternative equation that can be considered as a generalized Chasset-Thirion equation writing:

$$E(t) = E_{\infty}[1 + k(t/\tau_0)^{-m}] \qquad (5)$$

in which: $k = 1$ for positive strain steps ("UP", $\Delta\varepsilon > 0$)

$k = -1$ for negative strain steps ("DOWN", $\Delta\varepsilon < 0$) involving recovery.

Table 1 indicates that the exponent *m* is always positive except for CB-40-c (Equation 3). In order to take into account this particular case in Equation (5), one will add the following

condition: $k = -1$ when m is negative. E_∞ is the asymptotic equilibrium tensile modulus. Interestingly, for all samples (except CB-40-c), the asymptotic values E_∞(DOWN) are very close from E_∞(UP2) determined during the second step elongation.

The characteristic times τ_0 (Table 1) resulting from the fit vary considerably from sample to sample. In the present paper, τ_0 will be considered as a characteristic time scale but it will not be further discussed.

4.2. Experimental results obtained for $\varepsilon = 0.60$ and 0.80. The experimental results obtained for $\varepsilon = 0.60$ are plotted in Figure 5. In all cases, the spread of the curves UP1, DOWN and UP2 is narrower than it was for $\varepsilon = 0.40$ (Figure 4). For samples Si-OH-40-c, Si-OR-20-c and CB-40-c there are no DOWN plots because these samples were not strained above 0.60. For the other ones, the modified CT equation provides a good fit for the experimental data measured during the DOWN step. The CT equation fits well the UP1 and UP2 curves obtained for the two hydroxylated silica samples (Si-OH-20-c and Si-OH-40-c) and one of the hydrophobic silica sample (Si-OR-40-c). The values of the exponent m are indicated in brackets on figure 5. Concerning samples CB-20-c and CB-40-c (UP1), the best fit is obtained by a logarithmic equation:

$$E^*(t) = E(1)[1 - K \log(t)] \qquad (6)$$

The slope K is very similar and small (0.016 and 0.018, respectively) for both samples. Samples Si-OR-20-c and CB-40-c (UP2) behave as does CB-40-c (UP1) for $\varepsilon = 0.40$. m is negative and the data follow the generalized CT equation (Equation 5) with $k = -1$. However, the absolute values of the exponents m are smaller than it was for the smaller strain.

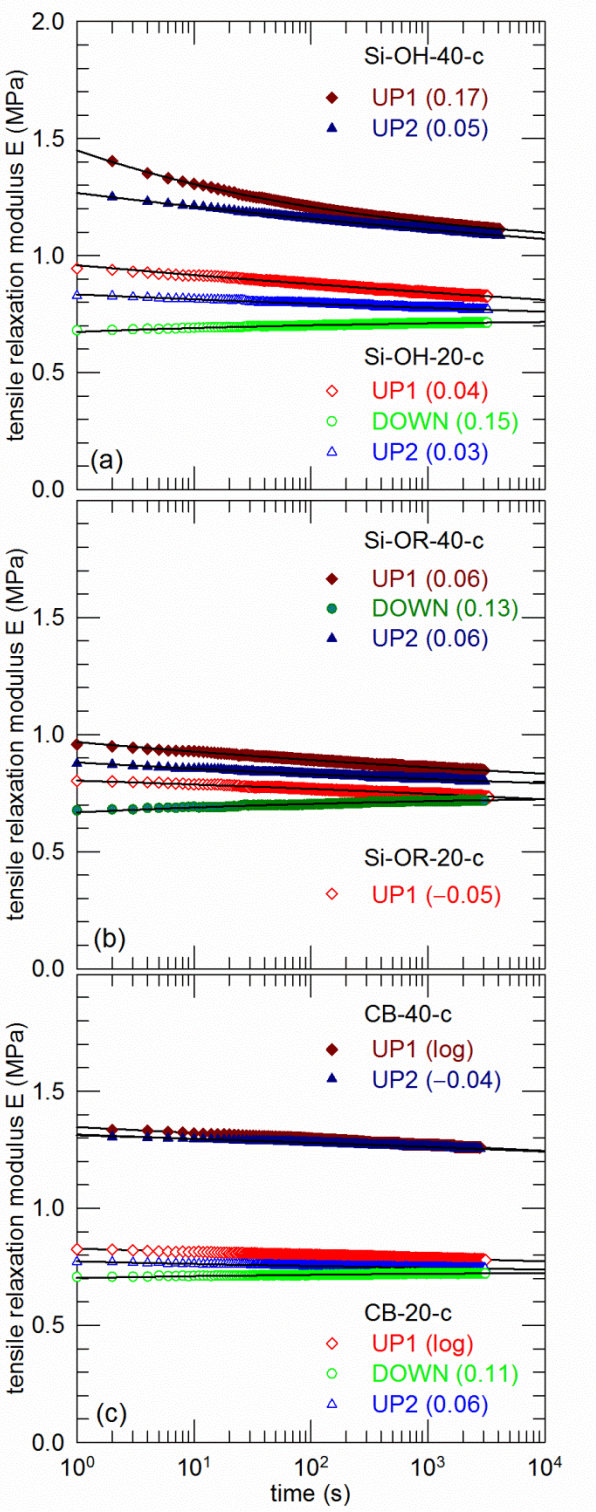

Figure 5. Time dependence of the tensile relaxation modulus E for ε = 0.60. The values of *m* are given in brackets.

The time dependence of the tensile relaxation modulus for $\varepsilon = 0.80$ is shown on figure 6. The amplitude of the diminution of $E(t)$ within the time window considered becomes quite small (the ordinate scale is amplified by a factor 2). For Si-OH-20-c (UP1) and Si-OR-40-c, the values of the exponent *m* (given in brackets on figure 6) deduced from the fit with the generalized CT equation (Equation 5) are nearly the same and quite small. A logarithmic decrease of $E(t)$ is observed for Si-OH-20-c (UP2) and for CB-20-c. The order of magnitude of the slopes (0.019 for the former and 0.016 and 0.011 for CB-20-c UP1 and UP2, respectively) are similar to that obtained for $\varepsilon = 0.60$.

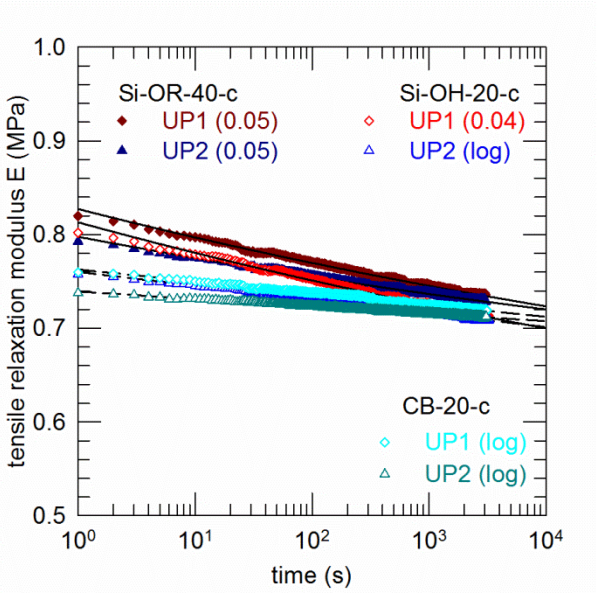

Figure 6. Time dependence of the tensile relaxation modulus E for ε = 0.80. The values of *m* are given in brackets.

4.3. Experimental results obtained for ε = 0.20. The shape of the curves plotted in figure 7 for ε = 0.20 (UP1 and UP2) is quite different from the previous ones measured at a larger strain. Most of them display a minimum located between 100 and 150 s followed by a domain in which $E(t)$ reaches a nearly constant value considered as being the asymptotic limit E_∞.

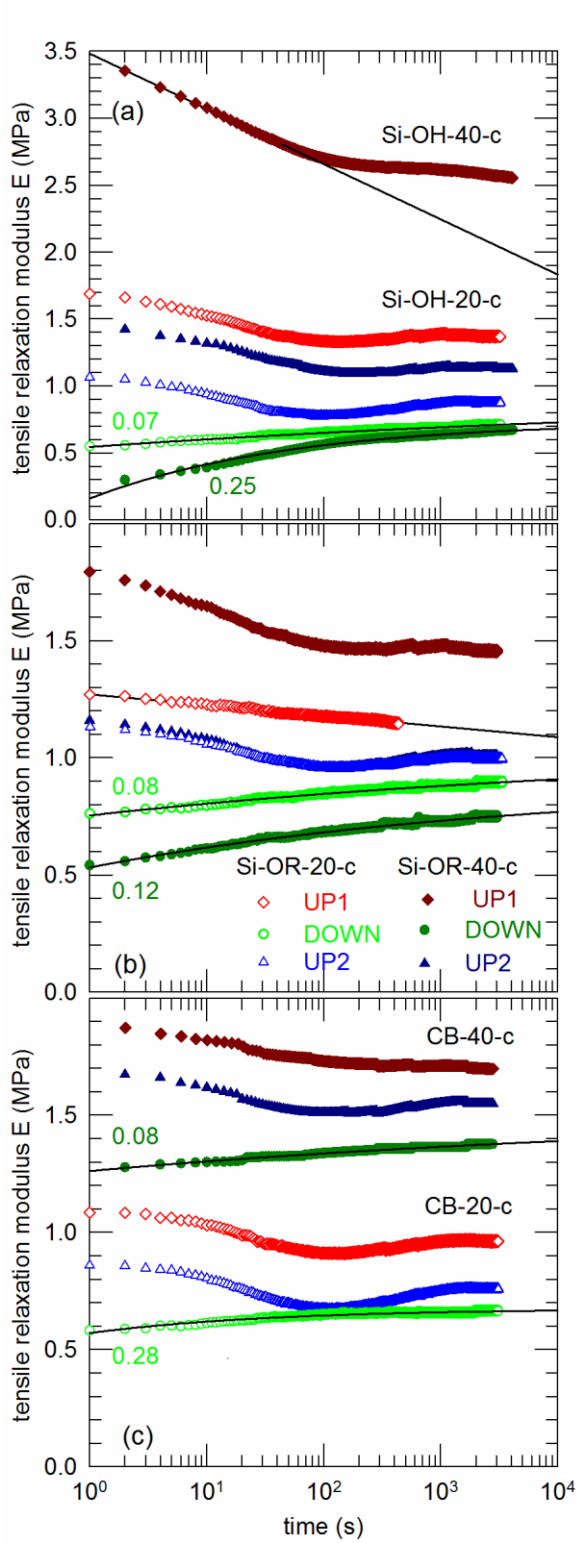

Figure 7. Time dependence of the tensile relaxation modulus E for ε = 0.20. The values of *m* obtained for the DOWN curves are indicated near each plot.

For sample Si-OH-40-c (UP1), the short time (t < 40 s) behavior can be described by a logarithmic decrease of $E(t)$. The slope K is equal to 0.118 which is significantly larger than it is for the samples at larger strains characterized by a logarithmic decrease of $E(t)$ over the whole time domain investigated. $E(1)$ is equal to 3.48 MPa. A logarithmic decrease of $E(t)$ is also observed for the sample Si-OR-20-c (UP1) in a larger range of time (up to 440 s). The slope is equal to 0.036 and $E(1)$ equals 1.27 MPa. For all other samples, the time dependence of the modulus at short times, up to the minimum, is nearly sigmoidal (in the semi-logarithmic representation). Existence of an initial fast decay of the relaxation modulus and a final slow decay at small strains was also reported in the case of carbon black filled natural rubbers or butadiene rubbers [20] or in carbon black filled EPDM elastomers [21]. The change of regime was often observed around 100 s as in the present case. At larger strains, the initial fast decay was no longer observed as also shown in Figures 4 to 6. Because this initial fast decay was not observed in un-filled rubbers, this feature was attributed by MacKenzie and Scalan [20] to a rapid re-formation of the filler network not completely destroyed at small strains.
Figure 7 show that the DOWN curves measured for ε = 0.20 are all well fitted by Equation (5) (in which $k = -1$) as for all DOWN curves obtained at larger strains.

4.3. Experimental results obtained for the uncross-linked Si-OH-40-u sample. Figure 8 shows the curves $E(t)$ obtained for this uncross-linked sample. It appears that their shape is very similar to that obtained for the corresponding cross-linked samples. For ε = 0.10, the tensile relaxation modulus decreases logarithmically with time over the same time interval (1 to 40 s) as for Si-OH-40-c sample (Figure 7a). $E(1)$ is equal to 3.33 MPa. The slope K = 0.189 is larger for this sample than for the cross-linked one but the strain is not the same (ε = 0.10 for the former

and 0.20 for the latter). For ε = 0.20 and above, the curves are well fitted by the CT equation. The values of the exponent *m* varying between 0.27 and 0.21, are slightly larger in the uncross-linked sample than in the cross-linked one. In the same way, the characteristic times τ_0 comprised between 0.5 and 3 seconds are significantly larger in the uncross-linked sample than in the cross-linked one. A similar result was also reported for natural and styrene-butadiene rubbers [24].

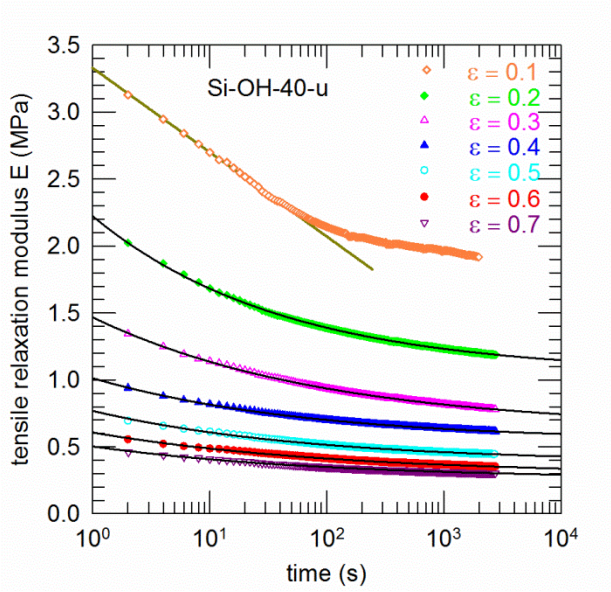

Figure 8. Time dependence of the tensile relaxation modulus E at different strains for the uncross-linked Si-OH-40 sample.

5. DISCUSSION

5.1. Physical meaning of the exponent *m* in the Chasset-Thirion equation

We have shown in the previous paragraph that all $E(t)$ data measured at a given strain ε larger than 0.20 and reached by increasing the elongation (UP curves) can be fitted by one of the following equations:

- the generalized Chasset-Thirion equation (Equation 5): $E(t) = E_\infty[1 + k(t/\tau_0)^{-m}]$

- a logarithmic equation (Equation 6): $\mathrm{E}(t) = E(1)[1 - K\log(t)]$

In both cases, the derivative which corresponds to the rate of change of the tensile modulus writes as:

$$|dE(t)/dt| \propto t^{-\alpha} \qquad (7)$$

with $\alpha = m + 1$ for the CT equation and $\alpha = 1$ for the logarithmic decrease (Equation 6). When α is smaller than 1, *m* is negative.

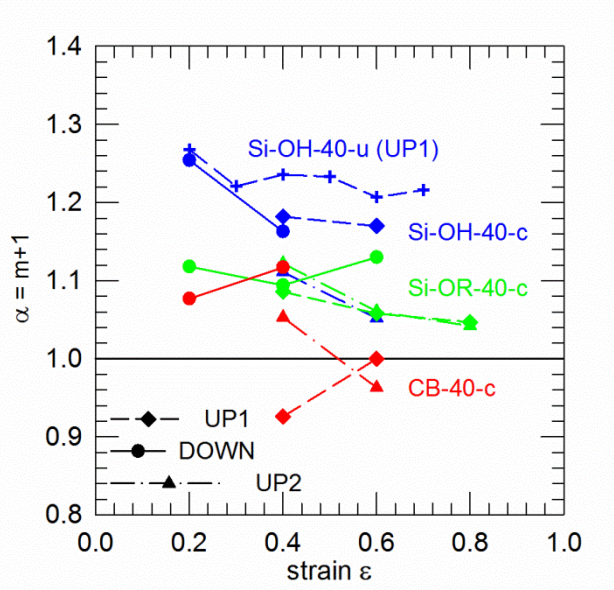

Figure 9. Comparison of the values of the exponent $\alpha = m + 1$ obtained at different strains.

The values of $\alpha = m + 1$ are plotted in figure 9 as a function of strain for the samples containing 40 phr of filler. This figure reveals the following trends:

- α is larger or close to 1.1 for the cross-linked hydroxylated silica samples (Si-OH-c) and larger than 1.2 for the uncross-linked one (Si-OH-u)

- α is smaller or close to 1.1 for the hydrophobic silica samples (Si-OR-c) and tends to 1 for the CB samples characterized by a log(*t*) decrease of tensile modulus

- α depends on the initial strain and on the filler-filler and filler-matrix interactions

- α is always strictly larger than 1 during recovery (DOWN).

As a consequence, the exponent α and, therefore, the CT exponent $m = \alpha - 1$ may be considered as a fingerprint of the time-dependent properties of strained viscoelastic materials. Within the approach of soft glass rheology (SGR) [39-41], the power law exponent generally labeled $(x - 1)$ characterizing the time-dependent viscoelastic properties is equal to 0 ($x = 1$) as the glass state is approached and to 1 ($x = 2$) for a viscous fluid. Our results suggest that the Chasset-Thirion exponent *m* is equivalent to the SRG exponent $(x - 1)$. In such conditions, α in equation (7) would correspond to *x* considered as an "effective noise temperature" [40] (also named "mechanical noise temperature"). In the present work, the value of the exponent *m* is not a characteristic of the material only but depends also on the strain (intensity and rate) and on its direction (UP or DOWN). As an example, for sample CB-20-c *m* is small (α = 1.04) for $\varepsilon = 0.40$ (UP1). For $\varepsilon = 0.60$ (UP1), the tensile relaxation modulus decreases as log(*t*) which corresponds to α = 1 in Equation(7). It is likely that this result can be interpreted as the strain induced jamming described by Wang and Robertson [77]. When the strain $\varepsilon = 0.60$ is reached in the decreasing step starting from $\varepsilon = 0.80$, $E(t)$ follows the generalized CT equation ($k = -1$) with an exponent $\alpha = 1.11$ (Figure 5). This feature agrees with the asymmetrical behavior discussed by these authors [77] already mentioned in §4.1. It suggests jamming resulting from the increase of the strain between 0.40 and 0.60 and unjamming when the strain is decreased from 0.80 to 0.60. More generally, we think that jamming could be revealed by the logarithmic time dependence corresponding to $\alpha = 1$ in Equation 7. In the SGR approach $x = 1$ indicates

that the system becomes close to the glassy state which would be reached at the at the glass transition temperature T_g of the plain unstrained elastomer. These features would agree with the concept of glassy bridges induced by strain in filled elastomers [14-16]. It agrees also with the increase of T_g observed in filled elastomers [59]. It should be mentioned, however, that the physical meaning of the words jamming and glass transition is not exactly the same [78]. Both words are used here within the scope of reference [77].

On the opposite, none of the silica filled samples exhibits this behavior, at least for strains ≤ 0.80 . The UP1 and the DOWN curves can all be fitted with the generalized CT equation. Accordingly, as shown in figure 9, the exponents α never reach the limit $\alpha = 1$. In the SRG model, it means that the system does not reach a glassy state under strain because *x* remains strictly above 1. This remark is in agreement with the absence of glassy domains observed in other silica filled elastomers [54-56]. More generally, the above comments agree with conclusions reached by Luo et al. [79] who combined NMR and mechanical measurements on silica-silane and carbon black filled styrene-butadiene rubber (SBR). Figure 9 also shows that the values of α are decreasing for the following filler sequence: hydroxylated silica, hydrophobic silica and carbon black. Interestingly, α is the largest for the uncross-linked sample filled with hydroxylated silica. In the SRG model, it means that the mechanical noise temperature *x* and, therefore, the chain mobility, decreases accordingly. This observation is consistent with the fact that cross-linking and/or filler matrix interaction decrease the chain mobility. It follows that one should have now the possibility to characterize the macroscopic dynamics in a filled system by means of an effective noise temperature *x* related to the polymer chain mobility that depends on the interaction with the filler particles and on the strain. Further experimental work would be necessary to examine the role of the morphology of the nanoparticles used as filler.

5.2. Analysis of the asymptotic limits. The determination of an asymptotic equilibrium by means of the CT equation allows us to examine the Mullins effect in these systems. To this end, we have plotted on Figure 10 and 11 the values of the stress $\sigma_0 = \varepsilon E(0)$ measured at $t = 0$ (Figure 2) and the values of $\sigma_\infty = \varepsilon E_\infty$ determined by means of the generalized CT equation for the three different fillers (40 phr). As expected, the second loading curves (UP2) are located between the first ones (UP1) and the unloading curves (DOWN). These figures show that the area of the hysteresis loop consisting of UP1 and DOWN curves decreases when going from Si-OH to Si-OR and to CB fillers (for 40 phr), i.e., when the filler matrix interaction increases. The magnitude of the hysteresis loop area seems similar for 40 phr (Figure 10c) and 20 phr (Figure 11b) of carbon black. In the case of hydroxylated silica, the decrease of the filler content seems to decrease the area of the hysteresis loop. This qualitative observation agrees with the Mullins effect model [80] based on dissipative friction phenomena due to internal sliding of the macromolecular chains and of the filler particles. It also intuitively agrees with the very different behavior of the filler particle velocity and relaxation investigated by HD-XPCS for Si-OH-40-c and CB-40-c ($\varepsilon = 0.60$) [51]. For Si-OH-40-c, the area of the hysteresis loop obtained by considering the asymptotic limits σ_∞ determined by means of the CT equation is significantly reduced. If the hysteresis observed for σ_0 would be related only to relaxation effects, no hysteresis would be expected for σ_∞. It follows that the hysteresis actually observed σ_∞ results from a modification of the silica particle network due to movements of the particles under strain and observed by XPCS. For CB-40-c (Figure 10c), the logarithmic decrease of the strain with time in the first loading does not yield an asymptotic limit. In this case it appears that the values of σ_∞ (DOWN) are very close to that obtained during the second loading (UP2). This feature is also observed for CB-20-c (Figure 11b).

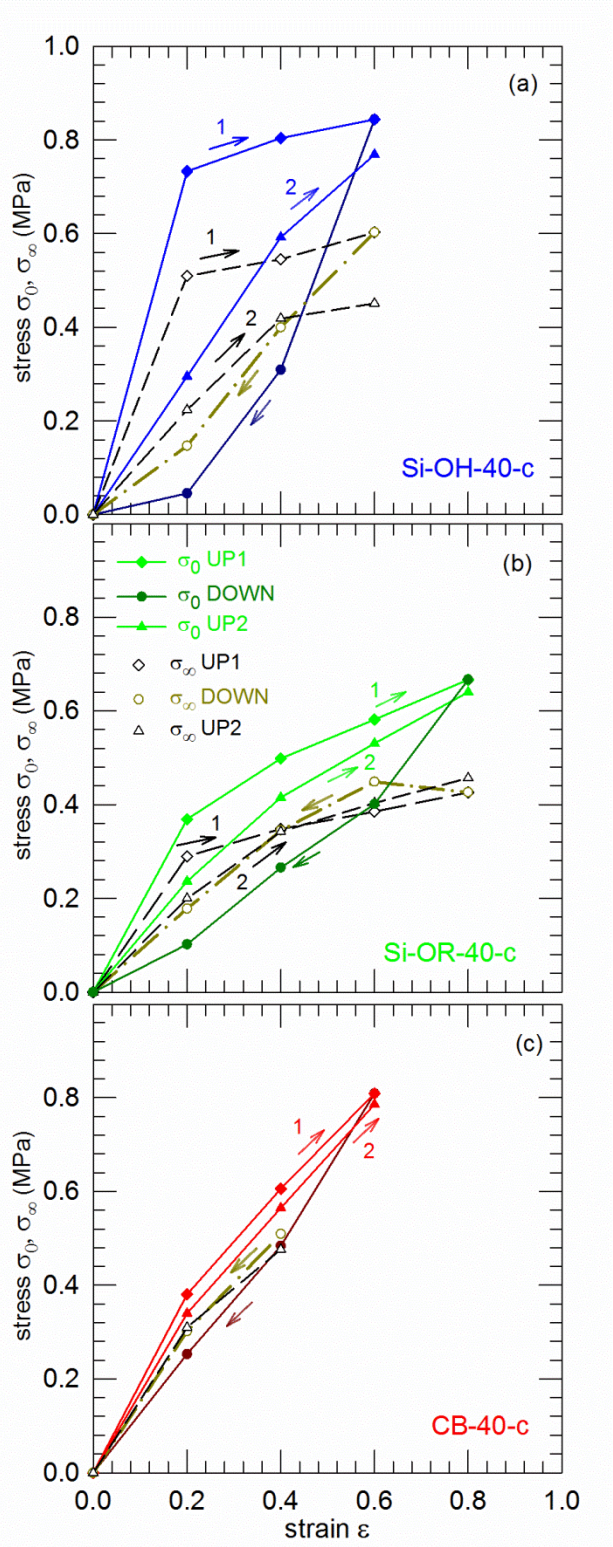

Figure 10. Evolution of the initial stress σ_0 and of the asymptotic limit σ_∞ determined by the CT equation: (a) the hydroxylated silica, (b) the hydrophobic silica and, (c) the carbon black fillers.

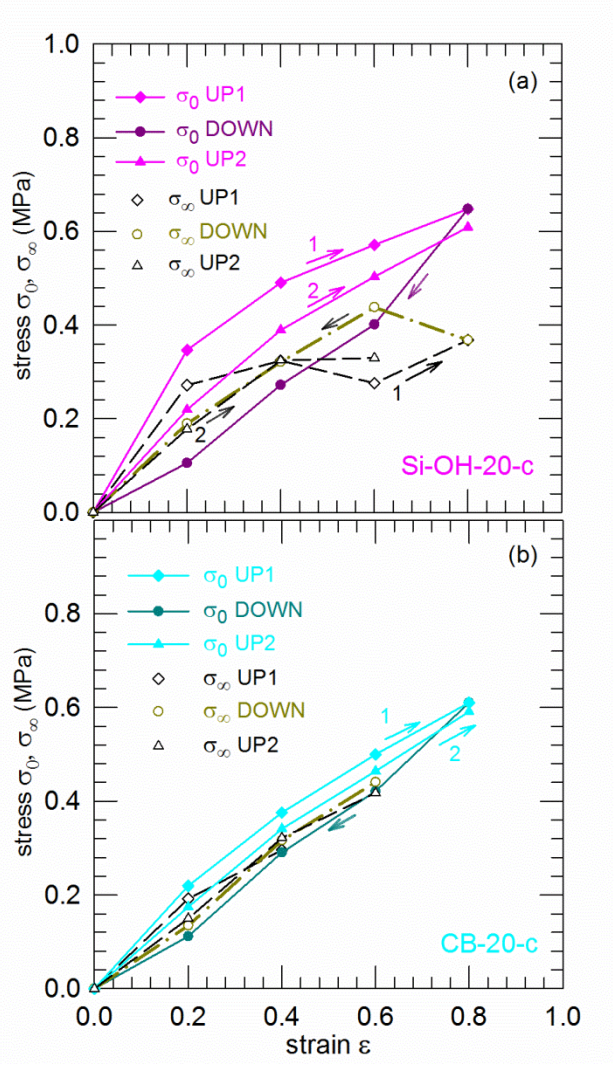

Figure 11. Evolution of the initial stress σ_0 and of the asymptotic limit σ_∞ determined by the CT equation: (a) the hydroxylated silica (20 phr) and, (b) the carbon black fillers (20 phr).

The shape of the σ_∞ hysteresis loop obtained for Si-OR-40-c (Figure 10b) and Si-OH-20-c (Figure 11a) is different: the UP1 and DOWN curves are crossing for $\varepsilon = 0.40$. It should be noticed that the upper strain was $\varepsilon = 0.80$ for these samples. Without additional experiments, it is difficult to discuss further these features. It appears, however, that for $\varepsilon \leq 0.40$ the values of

σ_∞ (DOWN) are very close to that obtained during the second loading (UP2) as it is the case for CB-40-c (Figure 10c) and CB-20-c.

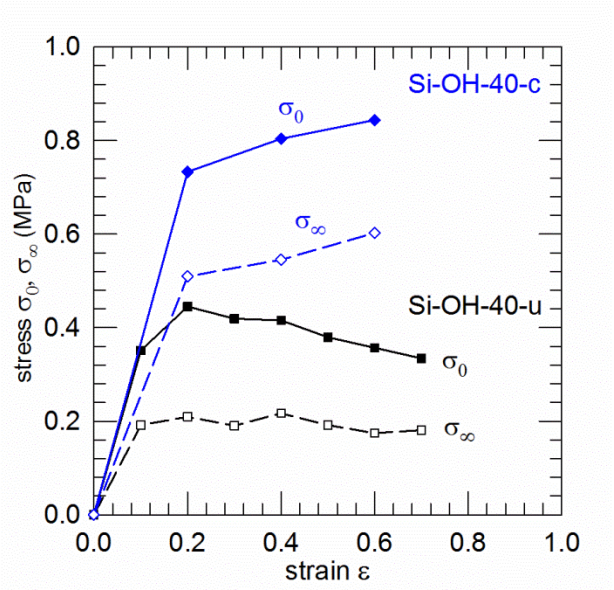

Figure 12. Comparison between the evolution of the initial stress σ_0 and the asymptotic limit σ_∞ for cross-linked (Si-OH-40-c) and uncross-linked (Si-OH-40-u) samples.

The effect of cross-linking on the evolution of σ_0 and σ_∞ with strain is reported in Figure 12 for the hydroxylated silica filler (Si-OH-40). For the uncross-linked sample Si-OH-40-u, σ_0 goes through a maximum at ε close to 0.20. Such a feature has already been observed for uncross-linked elastomers filled with silica or carbon black. It was shown to be coincident with the appearance of a "butterfly" in the SAXS patterns and attributed to the breaking and the reorganization of the colloidal particle network in the direction of the strain [62]. As discussed in the previous paragraph, the value of α are the largest for Si-OH-40-u which involves a larger chain mobility making possible the reorganization of the filler particle network. These features suggest that the generalized CT equation describes the breaking (or deflocculation) of the silica network and that this mechanism becomes independent of the strain above 0.20. The fact that the

asymptotic limit σ_∞ remains nearly constant suggests that the system tends to the same final deflocculated state.

6 SUMMARY AND CONCLUSION

In this study, we have first analyzed the stress-strain curves obtained according the standards procedure. The un-conventional plotting of the curves in logarithmic coordinates, allowed us to reveal the same non-linear stress-strain behavior for all samples. This feature suggests the occurrence of plastic events at small strain which could be similar to what was observed by simulations about the effect of tension in polymeric glasses. Therefore, it would be valuable to revisit, in the future, the analysis of previous experimental data.

The largest part of the study is dealing with the analysis of the behavior of the tensile relaxation modulus $E(t)$ at a given strain level reached either by a positive or a negative strain step. The leading parameter of this investigation was the filler-filler or the filler matrix interaction. We show that for all silica filled samples strained above 0.20 by a positive strain step, $E(t)$ follows the generalized Chasset-Thirion equation. For the carbon black samples characterized by a strong filler-matrix interaction the decrease of $E(t)$ is mainly logarithmic. These features indicate that the rate of decrease of $E(t)$ after a positive strain step follows a power law characterized by an exponent $\alpha = m + 1$. A similar feature is also observed for the rate of increase (recovery) of $E(t)$ after a negative strain step for all samples and at all strain plateaus including $\varepsilon = 0.20$. The values of m are always positive and the limiting case $m \to 0$ ($\alpha \to 1$) is never observed.

We have then remarked that the above power law features could be signatures of soft glassy rheology (SGR) phenomena characterized by a broad distribution of relaxation times and multiscale dynamical processes. It follows that (i) the exponent m involved in the Chasset-

Thirion equation would be equivalent to the exponent $x - 1$ involved in the SGR model and, (ii) the exponent $\alpha \equiv x$ could be considered as an effective noise temperature. In other words, one should have now the possibility to characterize the macroscopic dynamics in a filled system by means of an effective noise temperature *x* related to the polymer chain mobility that depends on the interaction with the filler particles and on the strain. We present several indications arising from the literature that may support this hypothesis. We think that the coming analysis of the series of HD-XPCS data obtained simultaneously with the mechanical measurements, and giving information about the "movements" of the filler particles, will be able to provide additional evidences of the pertinence of the SGR models in the field of filled elastomers.

Finally, the analysis of the limiting values (asymptotic limits) deduced from the fit of the data with the generalized CT equation, brings new information about the relative role of relaxation and plastic effect on the hysteresis (Mullins effect) observed in stress-strain measurements.

ACKNOWLEDGEMENTS

Use of the APS was supported by the DOE, Office of Basis Energy Sciences, under Contract No. W-31-109-Eng-38. The authors thank René Jurk (IFP Dresden) for the preparation of filled elastomers and for the measurement of the tensile stress-elongation curves.

REFERENCES

[1] Vilgis, T. A.; Heinrich, G.; Klüppel, M. Reinforcement of Polymer Nanocomposites: Theory, Experiments and Applications (Cambridge University Press, Cambridge, England, 2009).

[2] Heinrich, G.; Kaliske, M.; Lion, A.; Reese, S. *Constitutive Models for Rubber VI*;Taylor & Francis Group, London, UK, 2010.

[3] Roland, C. M. *Viscoelastic Behavior of Rubbery Materials*, Oxford University Press, Oxford, UK (2011); arXiv.org, e-Print Archive, Condensed Matter (2011), 1-46, arXiv:1104.1622v1 [cond-mat.soft].

[4] Thomas, S.; Stephen, R. *Rubber Nanocomposites: Preparation, Properties and Applications*; John Wiley & Sons (Asia) Pte Ltd Singapore 2010.

[5] Kumar, S. K.; Krishnamoorti, R. *Annu. Rev. Chem. Biomol. Eng.* **2010**, *1*, 37–58.

[6] Oberdisse, J.; Pyckhout-Hintzen, W.; Straube, E. Structure Determination of Polymer Nanocomposites by Small Angle Scattering. In *Recent Advances in Polymer Nanocomposites*; Thomas, S., Zaikov, G., Valsaraj, S. V., Eds.; Brill NV: Leiden, The Netherlands, 2009; p 397.

[7] Allegra, G.; Raos, G.; Vacatello, M. *Prog. Polym. Sci.* **2008**, *33*, 683–731.

[8] Drozdov, A. K.; Dorfmann, A. *Polym. Eng. Sci.* **2002**, *42*, 591-604.

[9] Chazeau, L.; Brown, J. D.; Yanyo, L. C.; Sternstein, S. S. *Polym. Compos.* **2000**, *21*, 202-222.

[10] Rendek, M.; Lion, A. *Z. Angew. Math. Mech.* **2010**, *90*, 436-458.

[11] Diani, J.; Fayolle, B.; Gilormini, P. *Eur. Polym. J.* **2009**, *45*, 601-612.

[12] Amin, A. F. M. S.; Lion, A.; Höfer, P. *Z. Angew. Math. Mech.* **2010**, *90*, 347-369.

[13] Bhattacharya, A.; Medvedev, G. A.; Caruthers, J. M. *Rubber Chem. Technol.* **2011**, *84*, 296-324.

[14] Merabia, S.; Sotta, P.; Long, D. R. *J. Polym. Sci.: Part B: Polym. Ph*ys. **2010**, *48*, 1495–1508.

[15] Papon, A.; Merabia, S.; Guy, L.; Lequeux, F.; Montes, H.; Sotta, P.; Long, D. R. *Macromolecules* **2012**, *45*, 2891−2904.

[16] Papon, A.; Montes, H.; Lequeux, F.; Oberdisse, J.; Saalwächter, K.; Guy, L. *Soft Matter* **2012**, *8*, 4090-4096.

[17] Bueche, F. *J. Appl. Polym. Sci.* **1960**, *4*, 107-114.

[18] Yan, L.; Dillard, D. A.; West, R. L.; Lower, L. D.; Gordon, G. V. *J. Polym. Sci. B* **2010**, *48*, 2207-2214.

[19] Yan, L.; Dillard, D. A.; West, R. L.; Rubis, K. J.; Gordon, G. V. *J. Polym. Sci. B* **2012**, *50*, 929-937.

[20] MacKenzie, C. I.; Scalan, J. *Polymer* **1984**, *25*, 559-568.

[21] Ginic-Markovich, M.; Dutta, N. K.; Dimopoulos, M.; Roy Choudhury, N.; Matisons, J. G. *Thermochim. Acta* **2000**, *357-358*, 211-216.

[22] Geethamma, V. G.; Pothen, L. A.; Rhao, B.; Neelakantan, N. R.; Thomas, S. *J. Appl. Polym. Sci.* **2004**, *94*, 96-104.

[23] Meera, A., P.; Said, S.; Grohens, Y.; Luyt, A. S.; Thomas, S. *Ind. Eng. Chem. Res.* **2009**, *48*, 3410-3416.

[24] Mitra, S.; Chattopadhyay, S.; Bhowmick, A. K. *J. Polym. Res*. **2011**, *18*, 489–497.

[25] Chasset, R.; Thirion, P. In *Proceedings of the Conference on Physics of Non-Crystalline Solids*; Prins, J. A. Ed.; North-Holland Publishing Co.: Amsterdam, 1965; p 345.

[26] Dickie, R. A.; Ferry, J. D. *J. Phys. Chem.* **1966**, *70*, 2594-2600.

[27] Batra, A.; Cohen, C.; Archer, L. *Macromolecules* **2005**, *38*, 7174-7180.

[28] Vega, D. A.; Villar, M. A.; Alessandrini, J. L.; Vallés E. M. *Macromolecules* **2001**, *34*, 4591-4596.

[29] Roth, L. E.; Vega, D. A.; Vallés E. M.; Villar, M. A. *Polymer* **2004**, *45*, 5923–5931.

[30] Martin, G.; Barrès, C.; Cassagnau, P.; Sonntag, P.; Garois, N. *Polymer* **2008**, *49*, 1892-1901.

[31] Joubert, C.; Michel, A.; Choplin, L.; Cassagnau, P. *J. Polym. Sci. B* **2003**, *41*, 1779-1790.

[32] Aniskevich, K.; Starkova, O.; Jansons, J.; Aniskevich, A. *Mech. Compos. Mater.* **2010**, *46*, 375-386.

[33] Curro, J. G.; Pincus, P. *Macromolecules* **1983**, *16*, 559-562.

[34] Curro, J. G.; Pearson, D. S.; Helfand, E. *Macromolecules* **1985**, *18*, 1157-1162.

[35] Heinrich, G.; Vilgis, T. A. *Macromolecules* **1992**, *25*, 404−407.

[36] Amir, A.; Oreg, Y.; Imry, Y. *Proc. Natl. Acad. Sci. U. S. A.* **2012**, *109*, 1850-1855.

[37] Jaishankar, A.; McKinley, G. H. *Proc. R. Soc. A* **2013**, *469*, 20120284.

[38] Rubinstein, M.; Obukhov, S. P. *Macromolecules* **1993**, *26*, 1740-1750.

[39] Sollich, P.; Lequeux, F.; Hébraud, P.; Cates, M. E. *Phys. Rev. Lett.* **1997**, *78*, 2020-2023.

[40] Sollich, P. *Phys. Rev. E* **1998**, *58*, 738-759.

[41] Fielding, S. M.; P. Sollich, P.; Cates, M. E. *J. Rheol.* **2000**, *44*, 323-369.

[42] Fabry, B.; Maksym, G. N.; Butler, J. P.; Glogauer, M.; Navajas, D.; Fredberg, J. J. *Phys. Rev. Lett.* **2001**, *87*, 148102.

[43] Alcarez, J.; Buscemi, L.; Grabulosa, M.; Trepat, X.; Fabry, B.; Farré, R.; Navajas, D. *Biophys. J.* **2003**, *84*, 2071-2079.

[44] Lenormand, G.; Millet, E.; Fabry, B.; James P. Butler, J. P.; Fredberg, J. J. *J. R. Soc. Interface* **2004**, *1*, 91-97.

[45] Trepat, X.; Lenormand, G.; Fredberg, J. J. *Soft Matter* **2008**, ***4, 1750-1759.***

[46] Mandadapu, K. K.; Govindjee, S.; Mofrad, M. R. K. *J. Biomech*. **2008**, *41* 1467–1478.

[47] Kollmannsberger, P.; Mierke, C. T.; Fabry, B. *Soft Matter* **2011**, *7*, 3127-3132.

[48] Balland, M.; Desprat, N.; Icard, D.; Féréol, S.; Asnacios, A.; Browaeys, J.; Hénon, S.; Gallet, F. *Phys. Rev. E* **2006**, *74*, 021911.

[49] Duenwald, S. E.; Vanderby Jr., R.; Lakes, R. S. *Ann. Biomed. Eng.* **2009**, *37*, 1131-1140.

[50] Hiratsuka, S.; Mizutani, Y.; Toda, A.; Fukushima, N.; Kawahara, K.; Tokumoto, H.; Okajima, T. *J. J. Appl. Phys.* **2009**, *48*, 08JB17.

[51] Ehrburger-Dolle, F.; Morfin, I.; Bley, F.; Livet, F.; Heinrich, G.; Richter, S.; Piché, L.; Sutton, M. *Macromolecules* **2012**, *45*, 8691-8701.

[52] Bonn, D.; Coussot, P.; , Huynh, H. T.; Bertrand, F.; Debrégeas, G. *Europhys. Lett.* **2002**, *5*, 786-792.

[53] Bandyopadhyay, R.; Liang, D.; Harden, J. L.; Leheny, R. L. *Solid State Commun*. **2006**, *139*, 589-598.

[54] Jouault, N.; Dalmas, F.; Said, S.; Di Cola, E.; Schweins, R.; Jestin, J.; Boué, F. *Phys. Rev. E* **2010**, *82*, 031801.

[55] Chevigny, C.; Jouault, N.; Dalmas, F.; Boué , F.; Jestin, J. *J. Polym. Sci., Part B* **2011**, *49*, 781-791.

[56] Jouault, N.; Dalmas, F.; Boué , F.; Jestin, J. *Polymer* **2012**, *53*, 761-775.

[57] Kraus G. *Angew. Makromol. Chem.* **1977**, *60-61*, 215-48.

[58] Pandey, Y. N.; Papakonstantopoulos, G. J.; Doxastakis, M. *Macromolecules* **2013**, *ASAP June 4.*

[59] Lin, C.-C.; Gam, S.; Meth, J. S.; Clarke, N.; Winey, K. I.; Composto, R. J. *Macromolecules* **2013**, *46*, 4502-4509.

[60] Rieker, T. P.; Hindermann-Bischoff, M.; Ehrburger-Dolle, F. *Langmuir* **2000**, *16*, 5588-5592.

[61] Ehrburger-Dolle, F.; Hindermann-Bischoff, M.; Geissler, E.; Rochas, C.; Bley, F.; Livet, F. *Mater. Res. Soc. Symp.* **2001**, *661*, KK7.4.1.

[62] Ehrburger-Dolle, F.; Bley, F.; Geissler, E.; Livet, F.; Morfin, I.; Rochas, C. *Macromol. Symp*. **2003**, *200*, 157-167.

[63] Hindermann-Bischoff, M.; Ehrburger-Dolle, F. *Carbon* **2001**, *39*, 375-382.

[64] Ehrburger, F.; Lahaye, J. *J. Phys. France* **1989**, *50*, 1349-1359.

[65] Dorigato, A.; Pegoretti, A.; Penati, A. *eXPRESS Polym. Lett.* **2010**, *4*, 115-129.

[66] Halloran, L. J. S. A Rheological Study of Stress Relaxation in Elastomers for in situ X-Ray Diffraction Measurements, Master Thesis, McGill University, Montreal, Quebec, Canada, January 20, 2011.

[67] Wilson, D. V. *J. Phys. D: Appl. Phys.***1974**, *7*, 954-968.

[68] Olofsson, J.; Larsson, D.; Svensson, I. L. *Metall. Mater. Trans. A* **2011**, *42A*, 3999-4007.

[69] Naik, N. K.; Perla, Y. *Polymer Testing* **2008**, *27*, 504-512.

[70] Weeks, A. A.; Sun, C. T. *Compos. Sci. Technol.* **1998**, *58*, 603-611.

[71] Tsai, J.; Sun, C. T. *Compos. Sci. Technol.* **2002**, *62*, 1289-1297.

[72] Papakonstantopoulos, G. J.; Riggleman, R. A.; Barrat, J.-L.; de Pablo, J. J. *Phys. Rev. E* **2008**, *77*, 041502

[73] Cheng, M.; Chen, W. *Internat. J. Solids Struct.* **2003**, *40*, 4749-4768.

[74] Heinrich, G.; Costa, F. R.; Abdel-Goad, M.; Wagenknecht, U.; Lauke, B.; Härtel, V.; Tschimmel, J.; Klüppel, M.; Svistkov, A. L. *Kautschuk Gummi Kunststoffe* **2005,** *58*, 163-167.

[75] Richter, S.; Saphiannikova, M.; Stöckelhuber, K. W.; Heinrich, G. *Macromol. Symp*. **2010**, *291–292*, 193–201.

[76] Richter, S.; Kreyenschulte, H.; Saphiannikova, M.; Götze, T.; Heinrich, G. *Macromol. Symp*. **2011**, *306-307*, 141–149.

[77] Wang, X.; Robertson, C. G. *Phys. Rev E* **2005**, *72*, 031406.

[78] Ikeda, A.; Berthier, L.; Sollich, P. *Phys. Rev. Lett*. **2012**, *109*, 018301.

[79] Luo H.; Klüppel M.; Schneider H. *Macromolecules* **2004**, *37*, 8000-8009.

[80] Cantournet, S.; Desmorat, R.; Besson, J. *Int. J. Solids Struct.* **2009**, *46*, 2255-2264.

For Table of Contents use only

Title: Tensile stress relaxation and recovery behavior of a cross-linked EPDM rubber matrix loaded with different fillers

Authors: Françoise Ehrburger-Dolle, Isabelle Morfin, Françoise Bley, Frédéric Livet, Gert Heinrich, Luc Piché, Mark Sutton

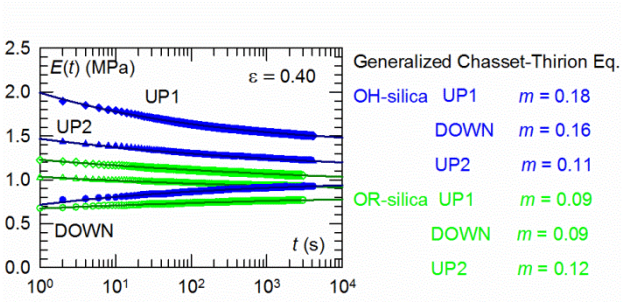

*Corresponding Author: Laboratoire Interdisciplinaire de Physique, 140 Avenue de la Physique, BP 87, 38402 Saint Martin d'Hères, France. Tel.: +33 476635880; Fax: +33 476635495; e-mail: francoise.ehrburger-dolle@ujf-grenoble.fr